Title

Mapping the Spatial Extent of Hypoperfusion in Chronic Thromboembolic Pulmonary Hypertension Using Multienergy CT.

Journal

Radiology Cardiothoracic Imaging, 5(4)

ISSN

2638-6135

Authors

Bird, Elizabeth

Hasenstab, Kyle

Kim, Nick

et al.

Publication Date

2023-08-01

DOI

10.1148/ryct.220221

Peer reviewed

Radiology: Cardiothoracic Imaging

ORIGINAL RESEARCH

Mapping the Spatial Extent of Hypoperfusion in Chronic Thromboembolic Pulmonary Hypertension Using Multienergy CT

Elizabeth Bird, BS • Kyle Hasenstab, PhD • Nick Kim, MD • Michael Madani, MD • Atul Malhotra, MD • Lewis Hahn, MD • Seth Kligerman, MD • Albert Hsiao, PhD • Francisco Contijoch, PhD

From the Department of Bioengineering (E.B., A.H., F.C.), Department of Radiology (K.H., L.H., S.K., A.H., F.C.), Department of Medicine, Division of Pulmonary, Critical Care, and Sleep Medicine (N.K., A.M.), and Department of Surgery (M.M.), University of California San Diego, 9500 Gilman Dr, MC 0412, La Jolla, CA 92093.
Received October 5, 2022; revision requested December 12; revision received June 5, 2023; accepted July 3. **Address correspondence to** F.C. (email: *fcontijoch@ucsd.edu*).

Supported by a GE Healthcare research grant, the National Institutes of Health (grant nos. HL143113 and HL158220), and a research grant from Bayer Healthcare.

Conflicts of interest are listed at the end of this article.

Radiology: Cardiothoracic Imaging 2023; 5(4):e220221 • https://doi.org/10.1148/ryct.220221 • Content codes: CH CT VA

Purpose: To assess if a novel automated method to spatially delineate and quantify the extent of hypoperfusion on multienergy CT angiograms can aid the evaluation of chronic thromboembolic pulmonary hypertension (CTEPH) disease severity.

Materials and Methods: Multienergy CT angiograms obtained between January 2018 and December 2020 in 51 patients with CTEPH (mean age, 47 years ± 17 [SD]; 27 women) were retrospectively compared with those in 110 controls with no imaging findings suggestive of pulmonary vascular abnormalities (mean age, 51 years ± 16; 81 women). Parenchymal iodine values were automatically isolated using deep learning lobar lung segmentations. Low iodine concentration was used to delineate areas of hypoperfusion and calculate hypoperfused lung volume (HLV). Receiver operating characteristic curves, correlations with preoperative and postoperative changes in invasive hemodynamics, and comparison with visual assessment of lobar hypoperfusion by two expert readers were evaluated.

Results: Global HLV correctly separated patients with CTEPH from controls (area under the receiver operating characteristic curve = 0.84; 10% HLV cutoff: 90% sensitivity, 72% accuracy, and 64% specificity) and correlated moderately with hemodynamic severity at time of imaging (pulmonary vascular resistance [PVR], $\rho = 0.67$; $P < .001$) and change after surgical treatment (ΔPVR, $\rho = -0.61$; $P < .001$). In patients surgically classified as having segmental disease, global HLV correlated with preoperative PVR ($\rho = 0.81$) and postoperative ΔPVR ($\rho = -0.70$). Lobar HLV correlated moderately with expert reader lobar assessment ($\rho_{HLV} = 0.71$ for reader 1; $\rho_{HLV} = 0.67$ for reader 2).

Conclusion: Automated quantification of hypoperfused areas in patients with CTEPH can be performed from clinical multienergy CT examinations and may aid clinical evaluation, particularly in patients with segmental-level disease.

Obstruction of the pulmonary arteries by chronic thromboembolism leads to chronic thromboembolic pulmonary hypertension (CTEPH) (1–3). Obstructions vary in number and location, leading to perfusion deficits in the pulmonary parenchyma, with varying spatial extent and spatial distributions. Agreement between location(s) of arterial obstructions, the extent and location of hypoperfusion, and the severity of pulmonary hypertension are important factors in diagnostic and treatment evaluations (4,5).

Multienergy CT pulmonary angiography offers a noninvasive approach to evaluate both arterial obstructions and hypoperfusion (6–12). Average global iodine concentration (termed *pulmonary blood volume* [PBV]) measured from iodine-water images is reduced in patients with acute pulmonary embolisms (PEs) and CTEPH (13). Additionally, reduced PBV in patients with CTEPH has also been correlated with hemodynamic severity (14–16). In addition to global assessment, PBV and multienergy CT pulmonary angiography iodine maps have proven useful in aiding the visual detection of individual perfusion deficits by expert readers (9,12,17). However, to date, iodine-water images have not been used to automatically delineate perfusion deficits in a pixelwise fashion and quantify the spatial extent of impairment.

The objective of this study was to further multienergy CT evaluation of pulmonary perfusion by developing and validating an automated quantitative approach to define, on a per-pixel basis, regions of hypoperfusion in patients with CTEPH. We assessed the agreement of the spatial extent of hypoperfusion measured with our approach with presurgical disease severity, changes in hemodynamics after surgical intervention, and expert radiologist visual assessment. We sought to determine if pixelwise evaluation can be particularly helpful in patients with chronic thromboembolic disease originating in the segmental pulmonary arteries.

Materials and Methods

Patient Selection

Under institutional review board–approved (approval no. 191797) waiver of informed consent and in compliance with the Health Insurance Portability and Accountability Act, 395 consecutive multienergy acquisitions obtained between January 1, 2018, and December 31, 2020, with

Abbreviations

AUC = area under the receiver operating characteristic curve, BMI = body mass index, CO = cardiac output, CTEPH = chronic thromboembolic pulmonary hypertension, HLV = hypoperfused lung volume, ICC = intraclass correlation coefficient, mPAP = mean pulmonary artery pressure, PAWP = pulmonary artery wedge pressure, PBV = pulmonary blood volume, PE = pulmonary embolism, PTE = pulmonary thromboendarterectomy, PVR = pulmonary vascular resistance, UCSD = University of California San Diego

Summary

Automated pixelwise delineation of hypoperfused lung areas from multienergy CT iodine images separated patients with chronic thromboembolic disease from controls and correlated with hemodynamics and expert visual assessment of hypoperfusion.

Key Points

- Global hypoperfused lung volume (HLV)—a novel automated pixelwise measure of the spatial extent of hypoperfusion throughout the lungs by using multienergy CT—separated patients with chronic thromboembolic pulmonary hypertension (CTEPH) from controls (area under the receiver operating characteristic curve = 0.84) and correlated with hemodynamic severity at time of imaging (pulmonary vascular resistance [PVR], ρ = 0.67; $P < .001$) and change in PVR after surgical treatment (ρ = −0.61, $P < .001$).
- In patients with CTEPH surgically classified as originating in the segmental vessels, global HLV correlated with hemodynamics, specifically with PVR before pulmonary thromboendarterectomy (ρ = 0.81, $P = .002$) and change in PVR after surgery (ρ = −0.70, $P = .01$).
- Lobar HLV correlated with expert visual assessment ($\rho_{reader1} = 0.71$, $\rho_{reader2} = 0.67$; $P < .001$ for both readers), with moderate agreement between readers (intraclass correlation coefficient = 0.61, $P < .001$).

Keywords

CT–Spectral Imaging (Multienergy), Pulmonary, Pulmonary Arteries, Embolism/Thrombosis, Chronic Thromboembolic Pulmonary Hypertension, Multienergy CT, Hypoperfusion

a single CT scanner were retrospectively evaluated (by author F.C., 12 years of experience in cardiovascular imaging) in an unmatched case-control fashion. Scans were acquired for the evaluation of CTEPH ($n = 120$) or suspicion of acute PE ($n = 275$) (Fig 1).

The CTEPH cohort (Fig 1) comprised patients who underwent pulmonary thromboendarterectomy (PTE) surgery for definitive treatment of CTEPH. Patient diagnosis and treatment selection were determined by consensus of a multidisciplinary team of cardiothoracic surgeons, vascular disease expert pulmonologists, and fellowship-trained cardiothoracic radiologists. Clinicians assessed CTEPH diagnosis by using the criteria from Galiè et al (2), which include mean pulmonary artery pressure (mPAP) greater than 25 mm Hg, pulmonary artery wedge pressure (PAWP) of 15 mm Hg or less, pulmonary vascular resistance (PVR) of 240 dyn·sec·cm^{-5} or greater, CTEPH-specific imaging signs, and ventilation-perfusion mismatch. Patients diagnosed with CTEPH were excluded if they did not undergo PTE (including those treated medically or by balloon pulmonary angioplasty), did not undergo preoperative multienergy imaging ($n = 65$), had a body mass index (BMI) greater than 50 kg/m^2 (which reduces image quality [18]; $n = 2$), or had automatic lobar segmentation measurements (see the Hypoperfused Lung Volume Assessment section) that failed visual inspection ($n = 2$; blinded visual review by author E.B., 5 years of experience in cardiovascular imaging). The final CTEPH cohort included 51 patients. Median time between multienergy CT imaging and PTE surgery was 5 days (43 of 51 within 30 days; range, 2–372 days). A subset of the patients with CTEPH ($n = 33$) had pre- and post-PTE invasive hemodynamic values available for review, which were used for comparison with CT-based evaluation (discussed in the Invasive Hemodynamics and Correlation with Perfusion section).

The control cohort comprised patients found to have no imaging findings suggestive of pulmonary vascular abnormalities after multienergy CT imaging was performed to rule out acute PE. Patients were excluded if the radiology report or patient medical record mentioned findings consistent with any PE (acute, subacute, or chronic; $n = 55$), pulmonary hypertension ($n = 26$), pulmonary veno-occlusive disease ($n = 4$), pulmonary artery sarcoma ($n = 4$), pneumothorax ($n = 3$), congenital heart disease ($n = 3$), pulmonary vein stenosis ($n = 2$), pulmonary arteriovenous malformation ($n = 1$), partial anomalous venous return ($n = 1$), or prior lobectomy ($n = 1$) (see Fig 1). As with the CTEPH cohort, studies were excluded for patient BMI greater than 50 kg/m^2 ($n = 28$), poor multienergy image quality (defined as pulmonary artery iodine signal-to-noise ratio < 10 [7], $n = 33$), or if automatic lobar segmentation failed visual inspection ($n = 5$). The final control cohort included 110 patients.

Image Acquisition

Multienergy CT pulmonary angiograms for both cohorts were acquired using the same multienergy protocol with one single-source Revolution CT scanner (GE Medical Systems). The acquisition rapidly switched kilovoltage peak (80 to 140 kVp), and data were acquired helically with an 80-mm detector width, median pitch of 1.38 (range, 0.98–1.38), and 0.5-second revolution time. Median tube current was 485 mAs (range, 240–630 mAs). Patients were administered iohexol contrast media (Omnipaque; GE Healthcare) with a concentration of 350 mg/mL based on BMI (BMI < 20: 60 mL at 4 mL/sec, BMI 20–29.9: 75 mL at 5 mL/sec, BMI 30–39.9: 80 mL at 5.5 mL/sec, BMI > 40: 90 mL at 6 mL/sec; median volume, 75 mL; range, 50–150 mL). Imaging was timed for pulmonary arterial phase imaging using SmartPrep bolus tracking software (GE Healthcare), with images acquired 8 seconds after main pulmonary artery enhancement at the T4 level reached 125 HU (19). Iodine-water material decompositions yielding iodine concentration in milligrams per milliliter were generated using the Gemstone Spectral Imaging software (GE Healthcare). All images were reconstructed on a 512 × 512 image grid with an xy resolution of 0.7 mm ± 0.1 (SD) (range, 0.5–0.9 mm) and section thickness of 1.25 mm. The typical field of view was 345 × 345 mm (range, 250–470 mm). Virtual

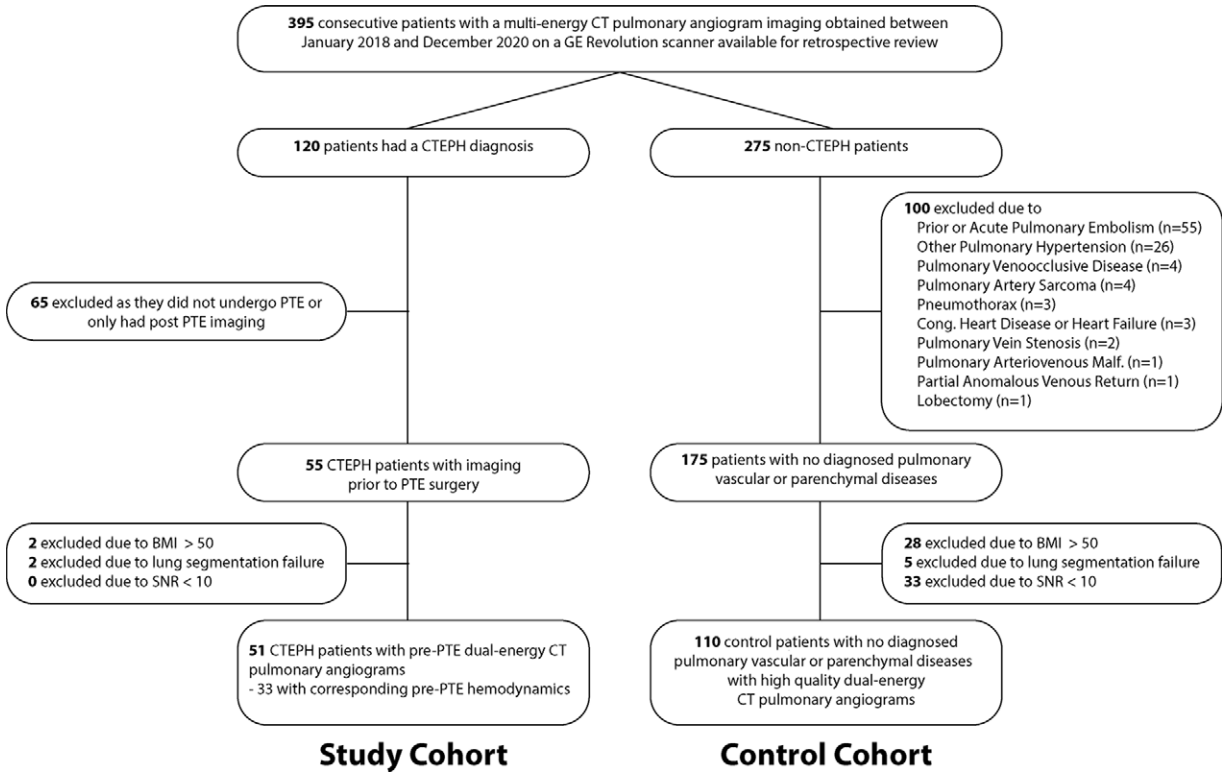

Figure 1: Flow diagram of study design. BMI = body mass index, Cong. = congestive, CTEPH = chronic thromboembolic pulmonary hypertension, CTPA = CT pulmonary angiography, Malf. = malformation, PTE = pulmonary thromboendarterectomy, SNR = signal-to-noise ratio.

monoenergetic images were reconstructed from the multienergy acquisition to simulate a 70 keV acquisition.

Hypoperfused Lung Volume Assessment

Pixelwise classification of the lung parenchyma as hypoperfused was obtained from the multienergy pulmonary angiograms to calculate metrics of global and lobar spatial hypoperfusion in a completely automated fashion. Automated processing generated iodine concentration maps for the lung parenchyma. First, lung lobes were automatically segmented from virtual monoenergetic images (Fig 2A, 2B) by using a recently published machine learning algorithm (20). The lobar segmentations were used to isolate the iodine signal (concentration in milligrams per milliliter) from iodine-water maps (Fig 2C), yielding lung parenchyma iodine concentration images (Fig 2D). The segmentation excluded large pulmonary vessels, bones, and airways, but smaller pulmonary vessels were removed separately. Specifically, pixels that were 2 SDs higher than the mean parenchymal concentration were removed. In addition, imperfect iodine-water separation (due to limited spectral separation of the incident x-ray beam, photon starvation, and artifacts from highly attenuating structures such as metal [21]) can lead to negative iodine concentrations independent of parenchyma perfusion, so pixels with iodine concentration −3 mg/mL or less were also removed.

After automated segmentation and isolation of the lung parenchyma iodine images, pixels with an iodine concentration ($I_{mg/mL}$) of 0 mg/mL or less (Fig 2E, blue pixels) were classified as hypoperfused. All other pixels were assigned a value of 0. This classification is shown in Equation 1 below:

$$f\left(I_{mg/mL}\right)=\begin{cases}1, I_{\frac{mg}{mL}} \le 0\,mg/mL\\ 0, I_{\frac{mg}{mL}} > 0\,mg/mL\end{cases} \quad (1).$$

Hypoperfused lung volume (HLV) was then calculated as the total number of hypoperfused parenchymal pixels divided by the total number of pixels (n) in the region of interest:

$$HLV=\frac{\sum_{i=1}^{n} f(I_{i,\,mg/mL})}{n} \quad (2).$$

In addition to global HLV, lobar HLV values (Fig 2F) were calculated by dividing the total number of hypoperfused pixels in each lobe by the volume of that lobe (and not the total lung volume). Therefore, global HLV represents a weighted average of the lobar HLV values.

For comparison, global PBV was measured according to the method described by Meinel et al (15), using the same iodine concentration images and segmentations used for HLV analysis. Briefly, 15% of the pulmonary artery iodine concentration was used to normalize parenchymal lung iodine concentrations. Mean pulmonary artery iodine concentration ($PA_{mg/mL}$) was measured for each patient by using a 4-cm^2 circular region of interest placed in the pulmonary artery trunk (drawn by author E.B.) using Horos open-source Digital Imaging and Communications in Medicine

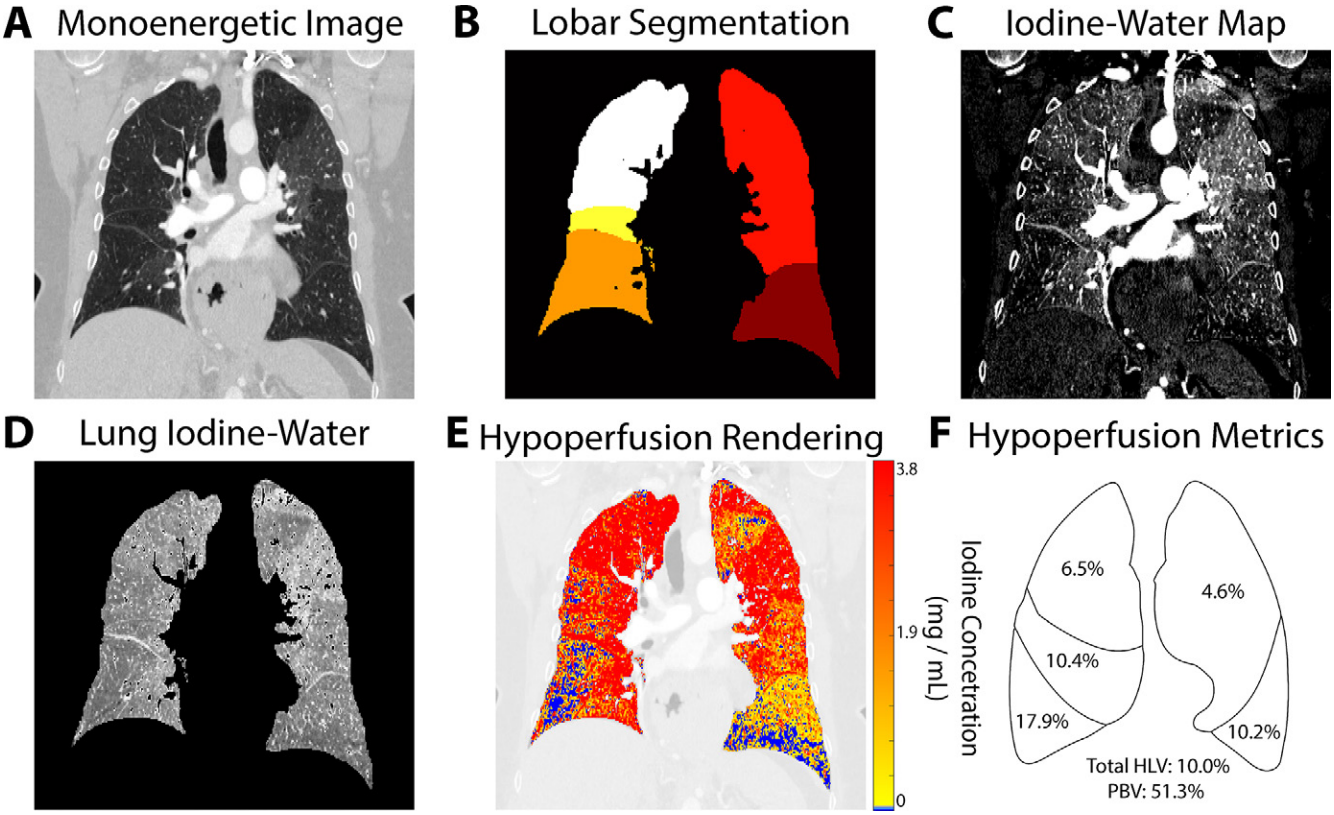

Figure 2: Automated segmentation and quantification of hypoperfused lung volume. CT angiograms generated **(A)** virtual monoenergetic images, which were **(B)** automatically segmented to identify lobar boundaries and remove other thoracic anatomy. These lobar segmentations were applied to **(C)** iodine-water images to **(D)** isolate the lung parenchyma. **(E, F)** Fused maps were then used to visualize **(E)** hypoperfused pixels, shown in blue, and quantify the percentage of hypoperfused pixels in each lobe **(F)**. A patient with chronic thromboembolic pulmonary hypertension with areas of hypoperfusion primarily in both lower lobes is shown as an example. HLV = hypoperfused lung volume, PBV = pulmonary blood volume.

viewer. This normalization by pulmonary artery iodine concentration yields a map of $I_{normalized}$ values as shown by Equation 3:

$$I_{normalized} = \frac{I_{mg/mL}}{0.15 \times PA_{mg/mL}} \quad (3).$$

Global PBV was then calculated as the average of $I_{normalized}$ over the whole normalized parenchymal lung (Eq 4), while lobar PBV was measured by averaging across an individual lobe:

$$PBV = \frac{\sum_{i=1}^{n} I_{i,\ normalized}}{n} \quad (4).$$

Equations 1–4 illustrate the similarities and differences between PBV and HLV. Specifically, HLV measures the fraction of a region of interest considered hypoperfused, while PBV is the spatial average of $I_{normalized}$. Thus, HLV reflects the extent of hypoperfusion at a given severity (or greater), while PBV averages together $I_{normalized}$ values from normal, hyperperfused, and hypoperfused areas.

Invasive Hemodynamics and Correlation with Perfusion

For most of the patients with CTEPH (44 of 51), systolic pressure, diastolic pressure, mPAP, and thermodilution-derived cardiac output (CO) before and after PTE surgery were obtained as part of routine clinical care. PVR was calculated preoperatively using right heart catheterization–measured PAWP according to the following equation: PVR = (mPAP − PAWP)/CO. Postoperative PVR was calculated using the central venous pressure to estimate PAWP, as PAWP is not measured by Swan-Ganz catheter in the intensive care unit at our institution (22). When multiple hemodynamics measurements were obtained, preoperative values obtained just before the PTE surgery and postoperative hemodynamics just prior to Swan-Ganz catheter removal were selected. Patient hemodynamics were excluded if they had a change in pulmonary hypertension medications after PTE surgery, to avoid the confounding effects of medications on the relationship between HLV and pulmonary hemodynamics. Eleven of the 44 patients with hemodynamics data had pulmonary hypertension medication changes after PTE. This resulted in a cohort of 33 patients with both pre- and post-PTE hemodynamics measurements without a change in pulmonary hypertension medications. The median time between hemodynamic recordings and imaging was 2 days, with 26 of 33 patients undergoing presurgical imaging within 30 days of hemodynamic recordings (range, 0–326 days). Median time between surgery and postoperative hemodynamics was 1 day (range, 0–8 days, Table 1).

Visual Assessment of Hypoperfusion and Comparison with HLV

Two fellowship-trained cardiothoracic radiologists (author S.K., with 13 years of post–cardiovascular radiology fellow-

Table 1: Characteristics of the CTEPH Cohort

Parameter	Value
Time between CT imaging and surgery (d)*	5 (3–8)
Time between preoperative hemodynamic recordings and CT (d)*	2 (1–24.5)
Time between postoperative hemodynamic recordings and surgery (d)*	1 (1–3)
Pre- and postoperative hemodynamic recordings	33 (65)
Pulmonary hypertension medication changes	11 (22)
NYHA functional class	
I	1 (2)
II	5 (10)
III	32 (64)
IV	4 (8)
Undefined	9 (21)
Disease level	
0	Right: 0 (0) Left: 3 (5.9)
1	Right: 17 (33.3) Left: 6 (11.8)
2	Right: 23 (45.1) Left: 25 (49.0)
3	Right: 11 (21.6) Left 17 (33.3)
4	Right: 0 (0) Left: 0 (0)
Hemodynamics	
mPAP (mm Hg)*	Before surgery: 45 (36–54) After surgery: 22 (18–26)
PVR (dyn·sec·cm–5)	Before surgery: 552 (346–758)* After surgery: 225 ± 108†
CO (L/min)†	Before surgery: 4.86 ± 1.53 After surgery: 5.75 ± 1.25

Note.—Unless otherwise noted, data are reported as numbers, with percentages in parentheses. CO = cardiac output, CTEPH = chronic thromboembolic pulmonary hypertension, mPAP = mean pulmonary artery pressure, NYHA = New York Heart Association, PVR = pulmonary vascular resistance.
* Data are reported as medians, with IQRs in parentheses.
† Data are reported as means ± SDs.

ship experience, and author L.H., with 3 years of post–cardiovascular radiology fellowship experience) blinded to HLV and PBV scores performed independent semiquantitative visual evaluation of hypoperfusion for all patients with CTEPH. Iodine-water images were reviewed and scored based on the percentage of each lobe considered to be hypoperfused. Readers were asked to categorize each lobe as having either no (0% of lobe affected), minimal (1% to <25% of lobe affected), mild (25% to <50% of lobe affected), moderate (50% to <75% of lobe affected), severe (75% to <100% of lobe affected), or complete (100% of lobe affected) hypoperfusion. Both readers had clinical experience evaluating CTEPH multienergy CT scans as attending radiologists at our institution but were not given specific instructions or training cases for this task.

Surgically Defined Segmental Disease Subgroup Analysis

The ability of HLV to help assess spatial hypoperfusion deficits in patients with chronic obstructions originating in the segmental pulmonary vasculature (surgically defined disease level 3) (5) was evaluated using classifications obtained during surgery. At the time of PTE surgery, each lung of each CTEPH case was classified as having disease located at the main pulmonary or lobar artery level (University of California San Diego [UCSD] surgical disease level classification 1 or 2), at the segmental level (UCSD surgical disease level classification 3), or at the subsegmental level (UCSD surgical disease level 4) by surgeons blinded to this analysis (5). The surgically defined segmental disease subgroup contained patients who had one or both lungs classified as having disease level 3. No patients in our cohort had disease level 4. Global HLV's performance in patients with surgically defined segmental disease and correlation with invasive hemodynamics, as well as lobar HLV's correlation with expert visual assessment, were measured. Of the 51 patients with CTEPH analyzed, 32 had surgically defined segmental disease. Of the 33 patients with CTEPH with complete hemodynamics data, 12 had surgically defined segmental disease.

Cases Series to Highlight the Clinical Use of HLV

Three cases are presented to demonstrate how HLV can capture known patterns of CTEPH impairment (n = 2) and how HLV can help identify patients with substantial obstructions despite high PBV (n = 1). For each case, a representative coronal section of the HLV map is presented alongside lobar scores, reader visual assessment scores, and the patient's subsequent surgical specimen.

Statistical Analysis

Demographic measures, image acquisition parameters, and invasive hemodynamics were tested for normality using the Shapiro-Wilks test. Normally distributed variables are reported as means ± SDs, and nonnormally distributed variables are reported as medians with IQRs (from Q1 to Q3) in parentheses. The Student t test and one-way analysis of variance were used to assess normally distributed variables, while Wilcoxon rank sum and Kruskal-Wallis tests were used for nonnormally distributed variables with P = .05. Receiver operating characteristic curves were used to identify both an HLV and PBV cutoff that best separated CTEPH scans from control scans. Given that the CTEPH cohort comprised patients with CTEPH necessitating surgical treatment, we evaluated global HLV and PBV cutoff performance at 90% sensitivity to minimize false-negative results. Receiver operating characteristic curves were compared using the Mann-Whitney statistic (23,24). Differences in global HLV and PBV cutoff specificity were compared with the McNemar test, while differences in accuracy were compared using z statistics (25). The agreement between global HLV and global PBV was determined via the Pearson correlation coefficient. Correlation of preoperative hemodynamics (mPAP, PVR, and CO) and postoperative change in hemodynamics (ΔmPAP, ΔPVR, and ΔCO) for both global HLV and PBV were also evaluated and compared using the Pearson correlation coefficient. Correlation between reader scores and lobar HLV for each reader was evaluated using the Spearman correlation coefficient. Forward multiple regression was performed to evaluate the complementary nature of HLV and PBV in predicting preoperative hemodynamics (mPAP, PVR, and CO). Correlations were classified as little to no relationship ($0 \le \rho < 0.25$), fair ($0.25 \le \rho < 0.5$), moderate ($0.5 \le \rho < 0.75$), or excellent ($\rho \ge 0.75$) (26). Correlation coefficients in dependent samples were compared using the t-score (27,28). Agreement between reader visual assessments was evaluated using intraclass correlation coefficient (ICC). ICCs were classified as little to no relationship ($0 \le$ ICC < 0.5), moderate ($0.5 \le$ ICC < 0.75), good ($0.75 \le$ ICC < 0.9), or excellent ($\rho \ge 0.9$) (29). Analysis was performed in MATLAB 2021a (MathWorks). Multiple regression was performed in SPSS Statistics (version 28.0.1.1; IBM). Statistics were performed by two of the authors (E.B. and F.C.).

Table 2: Summary of Control and CTEPH Cohort Patient Demographics

Parameter	Controls (n = 110)	CTEPH (n = 51)
Age (y)	51 ± 16	47 ± 17
Female sex	81 (73.6)	27 (52.9)*
BMI (kg/m^2)	39.2 ± 6.6	31.1 ± 7.5*
Race		
African American	5 (5)	12 (24)*
Asian	7 (6)	1 (2)
Pacific Islander	1 (1)	2 (4)
White	63 (57)	25 (49)
Indigenous, Alaska Native, or multiracial	33 (30)	11 (22)
Unknown	1 (1)	0 (0)

Note.—Data are reported as means ± SDs or numbers of patients, with percentages in parentheses. BMI = body mass index, CTEPH = chronic thromboembolic pulmonary hypertension.
* Statistically significant differences (P < .05).

Results

Patient Cohorts

The CTEPH cohort comprised 51 patients, and the control cohort comprised 110 patients. Controls and patients with CTEPH (Table 2) were similar in age (51 years ± 16 vs 47 years ± 17, respectively; P = .14). Patients with CTEPH had lower BMI than did controls (31.1 kg/m^2 ± 7.5 vs 39.2 kg/m^2 ± 6.6, respectively; P < .001), and more patients in the CTEPH cohort than in the control group self-identified as African American (n = 12, 24% vs n = 5, 5%; P = .03). The control group had more women (n = 78, 71% vs n = 27, 53%; P = .03). There was a significant difference in age of women versus men in the control cohort (48 years ± 16 vs 58 years ± 13, P = .01) and no evidence of a difference in the CTEPH cohort (44 years ± 16 vs 50 years ± 17, P = .17). For both cohorts, there was no evidence of differences between female and male patients in terms of BMI or race.

The cohort of patients with CTEPH had a mean preoperative mPAP of 45 mm Hg (IQR, 36–54 mm Hg), PVR of 552 dyn·sec·cm^{-5} (IQR, 346–758 dyn·sec·cm^{-5}), and CO of 4.86 L/min ± 1.53 (Table 1). PTE decreased median mPAP to 22 mm Hg (IQR, 18–26 mm Hg) and mean PVR to 225 dyn·sec·cm^{-5} ± 108 and increased mean CO to 5.75 L/min ± 1.25. The majority of patients with CTEPH were New York Heart Association Heart Failure Functional class III (n = 32, 64%) prior to PTE.

Right lungs had CTEPH surgical disease level 1 (n = 17, 33.3%), disease level 2 (n = 23, 45.1%), and disease level 3 (n = 11, 21.6%). Left lungs had CTEPH surgical disease level 0 (n = 3, 5.9%), disease level 1 (n = 6, 11.8%), disease level 2 (n = 25, 49.0%), and disease level 3 (n = 17, 33.3%). No patients had disease isolated to the subsegmental vasculature (level 4) in either the left or right lung.

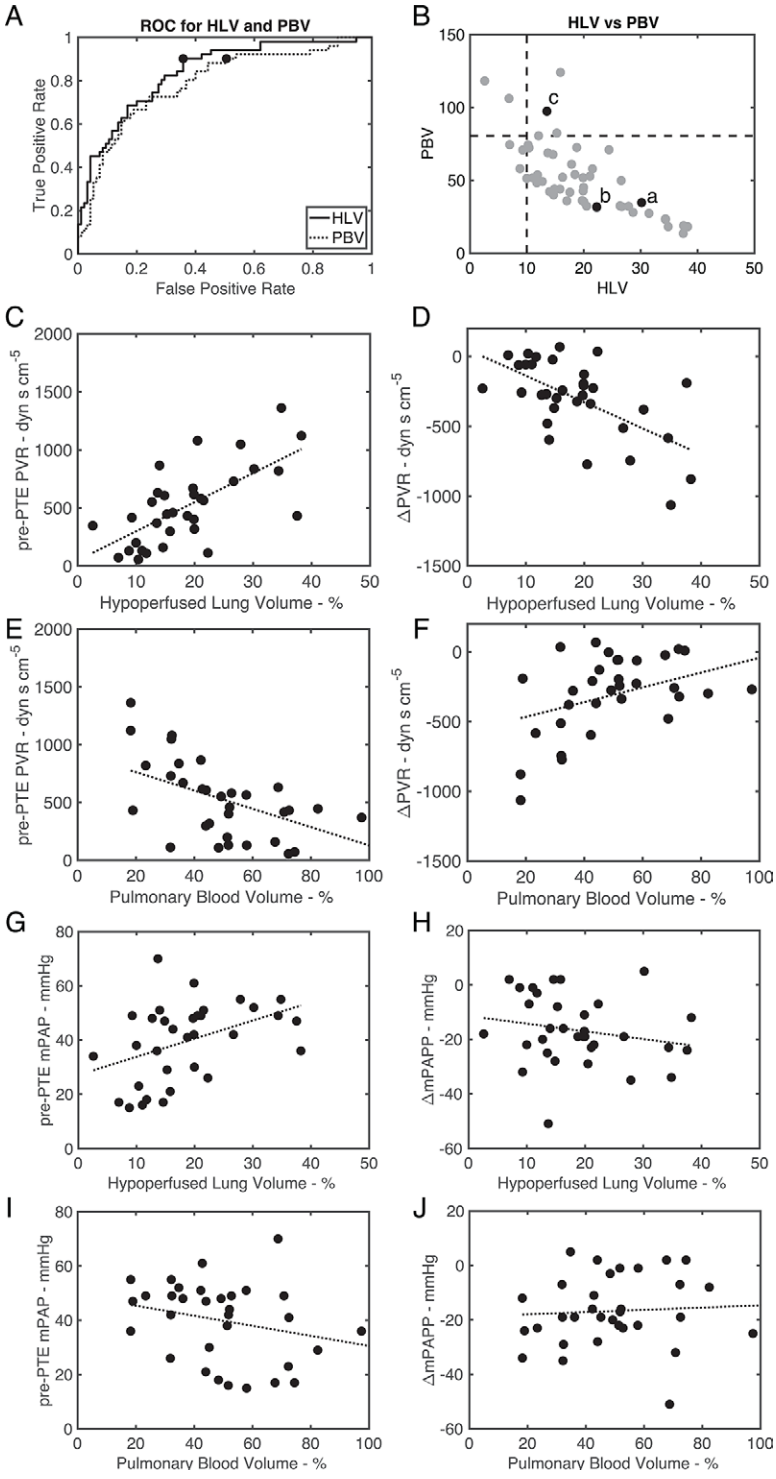

Figure 3: Agreement between multienergy metrics and correlation with hemodynamic assessment. **(A)** Global HLV (solid line) and mean PBV (dotted) distinguished CTEPH from controls (HLV AUC = 0.84 vs mean PBV AUC = 0.79, $P = .63$). Dots indicate 90% sensitivity cutoffs, which correspond to global HLV greater than 10.0% and global PBV less than 80.5%. **(B)** Global PBV and HLV are moderately correlated ($\rho = -0.72$, $P < .001$). Three of the five patients with CTEPH who had global PBV greater than 80.5% had elevated (>10%) global HLV (right upper quadrant). High sensitivity (>90%) cutoffs are shown as dotted lines. Dots labeled **a**–**c** are patients highlighted in Figures 4 and 5. **(C)** Global HLV significantly correlated ($\rho = 0.67$, $P < .001$) with pre-PTE PVR as well as **(D)** ΔPVR after PTE ($\rho = -0.61$, $P < .001$). **(E)** Global PBV significantly correlated ($\rho = -0.54$, $P = .001$) with pre-PTE PVR as well as **(F)** ΔPVR after PTE ($\rho = 0.43$, $P = .01$). **(G)** Global HLV ($\rho = 0.42$, $P = .02$), but not **(I)** PBV ($\rho = -0.29$, $P = .10$), significantly correlated with preoperative mPAP. **(H)** ΔmPAP after PTE surgery was not significantly correlated with global HLV ($\rho = -0.20$, $P = .27$) or **(J)** PBV ($\rho = 0.07$, $P = .68$). AUC = area under the ROC curve, CTEPH = chronic thromboembolic pulmonary hypertension, HLV = hypoperfused lung volume, mPAP = mean pulmonary artery pressure, PBV = pulmonary blood volume, PTE = pulmonary thromboendarterectomy, PVR = pulmonary vascular resistance, ROC = receiver operating characteristic.

Quantification of HLV and Comparison with PBV

Global HLV (area under the receiver operating characteristic curve [AUC] = 0.84 [95% CI: 0.81, 0.87]) and PBV (AUC = 0.79 [95% CI: 0.75, 0.82]) separated patients with CTEPH from controls (Fig 3A). Detection of CTEPH cases from controls with 90% (46 of 51) sensitivity corresponded to global HLV greater than 10% and global PBV less than 80.5%. Global HLV greater than 10% had 72% (116 of 161) accuracy and 64% (70 of 110) specificity. Global PBV less than 80.5% had similar accuracy (63%, 102 of 161; $P = .10$) but significantly lower specificity (51%, 56 of 110; $P < .001$) (Table 3). Global HLV and PBV had a moderate negative correlation ($\rho = -0.72$, $P < .001$) (Fig 3B). Of the five patients with CTEPH with global PBV within the normal range (>80.5%), three had global HLV indicating disease (HLV > 10%). Surgery led to a sizeable decrease in PVR (range, 237–298 dyn·sec·cm^{-5}) in these three patients.

Correlation of Hypoperfusion Metrics with Hemodynamics

Preoperative PVR correlated moderately with global HLV ($\rho = 0.67$, $P < .001$) and mean PBV ($\rho = -0.54$, $P = .001$) (Table 4). Similarly, ΔPVR after PTE correlated moderately with global HLV ($\rho = -0.61$, $P < .001$) and fairly with PBV ($\rho = 0.43$, $P = .01$) (Fig 3C–3F). Although a better degree of correlation was observed with global HLV compared with PBV, the *t*-score associated with this difference did not reach statistical significance for either preoperative PVR ($P = .15$) or ΔPVR ($P = .08$) metrics.

Preoperative mPAP correlated fairly with global HLV ($\rho = 0.42$, $P = .02$) and showed no correlation with PBV ($\rho = -0.29$, $P = .10$). Neither global HLV ($\rho = -0.20$, $P = .27$) nor PBV ($\rho = 0.07$, $P = .68$) was correlated with ΔmPAP after surgery (Fig 3G–3J). Correlation of preoperative CO with global HLV ($\rho = -0.52$, $P = .002$) and PBV ($\rho = 0.37$, $P = .03$) were not different ($P = .16$). Likewise, ΔCO after surgery was not correlated with global HLV ($\rho = 0.45$, $P = .14$) or PBV ($\rho = 0.1$, $P = .76$).

The addition of PBV to a linear regression using HLV (via forward multiple linear regression) did not improve model performance for PVR ($P = .85$), mPAP ($P = .76$), CO ($P = .75$),

Table 3: Separation of Patients with CTEPH and Controls Using Global HLV and PBV

Metric	AUC	Threshold	Accuracy	Sensitivity	Specificity
HLV	0.84	>10.0%	116/161 (72%)	46/51 (90%)	70/110 (64%)
PBV	0.79	<80.5%	102/161 (64%)	46/51 (90%)	56/110 (51%)
P value	.63	NA	.10	NA	<.001

Note.—At a 90% sensitivity operating point, HLV had higher specificity ($P < .001$) than did PBV. AUC = area under the receiver operating characteristic curve, HLV = hypoperfused lung volume, NA = not applicable, PBV = pulmonary blood volume.

Table 4: Correlation of Global HLV and PBV with Preoperative Hemodynamics and Change in Hemodynamics after Surgical Treatment

	HLV		PBV	
Patients	ρ Value	*P* Value	ρ Value	*P* Value
All patients with hemodynamics data (*n* = 33)				
Preoperative				
PVR	0.67	<.001	−0.54	.001
mPAP	0.42	.02	−0.29	.10
CO	−0.52	.002	0.37	.03
Change after surgery				
ΔPVR	−0.61	<.001	0.43	.01
ΔmPAP	−0.20	.27	0.07	.68
ΔCO	0.32	.07	−0.03	.85
Only those with segmental disease (*n* = 12)				
Preoperative				
PVR	0.81	.002	−0.48	.12
mPAP	0.43	.16	−0.17	.60
CO	−0.80	.002	0.54	.07
Change after surgery				
ΔPVR	−0.70	.01	0.31	.33
ΔmPAP	−0.29	.37	0.00	.99
ΔCO	0.45	.14	0.1	.76

Note.—Correlation of HLV and PBV with PVR and CO were not significantly different ($P = .15$ and $P = .16$, respectively). In patients with segmental disease, only HLV and not PBV had significant correlation with PVR, ΔPVR, and CO. CO = cardiac output, HLV = hypoperfused lung volume, mPAP = mean pulmonary artery pressure, PBV = pulmonary blood volume, PVR = pulmonary vascular resistance.

or ΔPVR ($P = .68$). Of note, there were significant correlations between preoperative hemodynamics, specifically, PVR and mPAP ($\rho = 0.72$, $P < .001$) and PVR and CO ($\rho = -0.76$, $P < .001$). However, mPAP and CO were not significantly correlated ($\rho = -0.32$, $P = .07$).

Expert Visual Assessment of Lobar Hypoperfusion and Comparison with Lobar HLV

For visual assessment, 255 lobes (51 patients with CTEPH, each with five lung lobes scored) were independently assessed by each reader. Reader 1 identified 247 of 255 lobes as hypoperfused (16 minimal, 27 mild, 82 moderate, 93 severe, and 29 complete hypoperfusion) in the CTEPH cohort (Fig 4A), while reader 2 identified 225 of 255 lobes as hypoperfused (31 minimal, 46 mild, 58 moderate, 65 severe, and 25 complete hypoperfusion) (Fig 4B). The HLV of lobes graded as completely, severely, moderately, and mildly hypoperfused were significantly different ($P < .001$) for both expert readers.

Visual assessments by reader 1 and reader 2 correlated moderately with lobar HLV ($\rho = 0.71$ and $\rho = 0.67$, $P < .001$ for both) and moderately with lobar PBV ($\rho = -0.57$ and $\rho = -0.68$, $P < .001$ for both). For reader 1, visual assessment was more strongly correlated with lobar HLV than with PBV (*t*-statistic = 5.2, $P < .001$). For reader 2, there was no evidence of a difference between correlations for lobar HLV and PBV (*t*-statistic = −0.29, $P = .61$). Agreement between the two readers was moderate, with an ICC of 0.61 ($P < .001$); 60% (133 of 255) of lobes had matching classifications (Fig

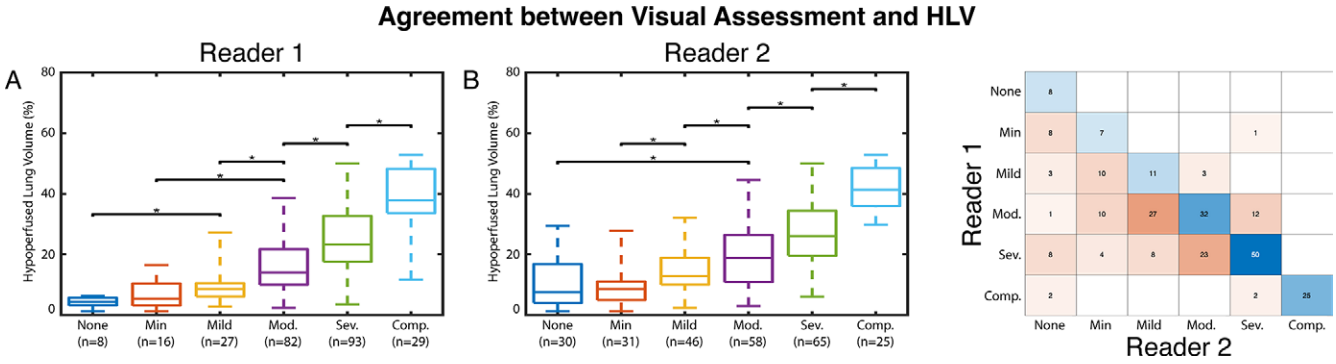

Figure 4: Agreement between lobar HLV percentage of hypoperfusion and lobar hypoperfusion severity scores from expert radiologists. Expert reader visual hypoperfusion assessment resulted in lobe hypoperfusion classifications with statistically different lobar HLV scores for complete, severe, moderate, and mild hypoperfused lobes ($P < .001$). * indicates significant differences ($P \leq .007$, Bonferroni correction for multiple comparisons) between different individual visual assessment groups. **(A)** Reader 1 lobar hypoperfusion scores were moderately correlated ($\rho = 0.71$, $P < .001$) with lobar HLV and lobar PBV ($\rho = -0.57$, $P < .001$), with stronger correlation with lobar HLV than with PBV (*t*-statistic = 5.2, $P < .001$). **(B)** Reader 2 lobar hypoperfusion scores were moderately correlated ($\rho = 0.67$, $P < .001$) with lobar HLV and lobar PBV ($\rho = 0.68$, $P < .001$). Lobar HLV and PBV had similar correlation strengths with reader 2 visual assessment (*t*-statistic = −0.29, $P = .61$). Boxes represent the IQR (25th–75th percentile), the horizontal lines inside the boxes represent the median values, and the whiskers represent the minimum and maximum values. **(C)** Confusion matrix shows agreement between reader 1 and reader 2. Exact agreement occurred in 60% (133 of 255) of lobes, and 85% (218 of 255 lobes) had reader assignments that were the same or within one hypoperfusion severity grade. Of the 37 disagreements of more than one grade, 36 occurred in lobes that reader 2 identified as having no to mild hypoperfusion. Comp. = complete, HLV = hypoperfused lung volume, Min. = minimal, Mod. = moderate, Sev. = severe.

4C), and 85% (218 of 255 lobes) had reader scores within one grade. Of the 37 disagreements of more than one grade, 36 occurred in lobes that reader 2 identified as having none to mild hypoperfusion.

Surgically Defined Segmental Disease Subgroup Analysis

Separation of patients with CTEPH surgically defined as level 3 (originating in segmental vessels) (n = 19) from controls had similar performance as the overall CTEPH cohort. A global HLV threshold of greater than 10.0% led to a sensitivity of 95% (18 of 19) and an accuracy of 67% (87 of 129), which did not differ from the sensitivity (P = .52) or accuracy (P = .67) found for the overall CTEPH cohort. Global PBV threshold of less than 80.5% led to a sensitivity of 95% (18 of 19) and an accuracy of 57% (73 of 129), with both values similar to those found for patients with CTEPH of any disease level (sensitivity, P = .52; accuracy, P = .56). Global HLV and PBV correlated moderately (ρ = −0.71, P < .001) in patients with surgically defined segmental CTEPH, which agreed (P = .96) with the correlation observed in the overall CTEPH cohort.

In patients with segmental disease and invasive hemodynamics (n = 12), global HLV strongly correlated with preoperative PVR (ρ = 0.81, P = .002) and moderately correlated with ΔPVR after PTE (ρ = −0.70, P = .01) (Table 4). Global PBV did not significantly correlate with any hemodynamics in patients with segmental disease.

Visual assessment of surgically defined segmental CTEPH moderately correlated with lobar HLV for reader 1 (ρ = 0.68, P < .001) and reader 2 (ρ = 0.63, P < .001). These correlation coefficients were similar to those calculated for visual assessment for all disease levels (reader 1: P = .54, reader 2: P = .36). Similarly, the correlation of lobar PBV with visual assessment in segmental CTEPH (reader 1: ρ = −0.49, P < .001; reader 2: ρ = −0.60, P < .001) was similar to that of the overall CTEPH cohort (reader 1: P = .56, reader 2: P = .21).

Example Cases

Example cases (labeled as a–c in Fig 3B) were chosen to highlight the use of HLV in specific clinical scenarios. Patient A in Figure 5 has bilateral, predominantly lower lobe hypoperfusion, while patient B presents with a unilateral pattern of disease. Both patients have similar global PBV values (A: 34.7%, B: 31.8%) but differ in their global HLV (A: 30.2%, B: 22.3%) and lobar HLV values. Readers 1 and 2 agreed on the visual evaluation of both patients, and the rank order for the reader scores matches the rank order for the lobar HLV scores in all lobes except the left upper lobe of patient A.

Figure 6 demonstrates findings in a patient who had a global PBV of 97.4% (normal, >80.5%) despite having hemodynamic impairment and a removed surgical specimen. This patient had a global HLV of 13.5% (>10.0% cutoff). The readers agreed on the severity of hypoperfusion of the lobes relative to one another, but reader 1 graded the hypoperfusion as more severe than did reader 2.

Discussion

We have developed and validated an automated, quantitative approach to define, on a per-pixel basis, regions of hypoperfusion in patients with CTEPH by using multienergy CT and evaluated its potential clinical use. The developed metric, global HLV, correctly classified patients with CTEPH and controls (AUC = 0.84) and had higher specificity relative to global PBV (64% vs 51%). Global HLV correlated with PVR at the time of imaging (preoperatively, ρ = 0.67) and predicted change in PVR after surgery in the entire cohort (ρ = −0.61), as well as in the subset of patients who had surgically defined segmental disease (ρ = −0.70). Lobar HLV agreed with visual assessment by two expert radiologists (ρ = 0.71 and ρ = 0.67).

Throughout the article, HLV findings are presented alongside a previously published multienergy-based measurement of global mean lung parenchymal perfusion (PBV) (8,9,14–16).

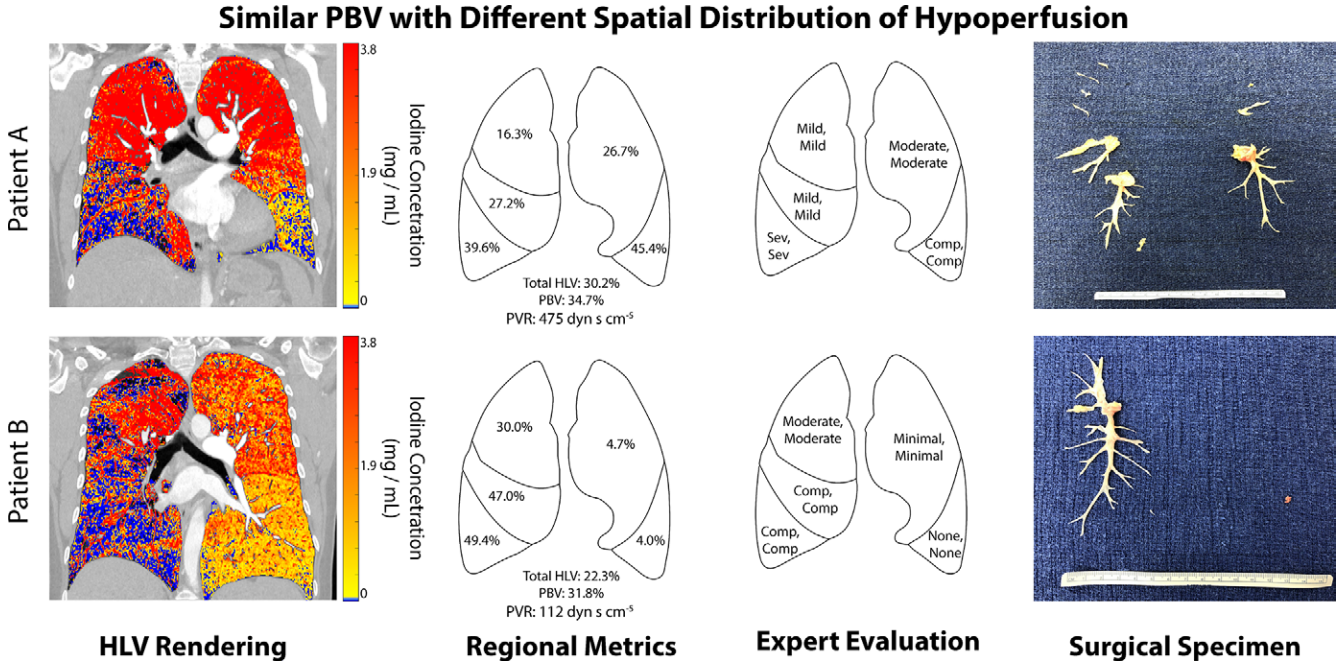

Figure 5: Use of HLV to characterize spatial patterns of chronic thromboembolic regional perfusion deficits. Patients A and B had surgical specimens that indicate a different distribution of disease (patient A: bilateral lower lobe disease, patient B: unilateral right lung pattern) despite similar level of global impairment (PBV = 34.7% and 31.8%, respectively). Global HLV identified a different extent of impaired lung volume (HLV: 30.2% vs 22.3%). In addition, for patient A, lobar HLV assessment shows extensive hypoperfusion (blue on HLV mapping) bilaterally (left lobes: 26.7%–45.4%, right lobes: 16.3%–39.6%), with extensive impairment in both lower lobes (left: 45.4%, right: 39.6%). Both expert reader assessments agreed with lobar HLV and scored the left and right lower lobes with the most severe hypoperfusion (complete and severe, respectively). Lobar HLV evaluation in patient B supports the unilateral pattern of disease (right lobes: 30.0%–49.4% vs left lobes: 4.0%–4.7%). Expert assessment also supported the unilateral disease pattern, with both readers classifying all lobes of the right lung with more severe hypoperfusion than the left lung. Comp = complete, HLV = hypoperfused lung volume, PBV = pulmonary blood volume, PVR = pulmonary vascular resistance, Sev = severe.

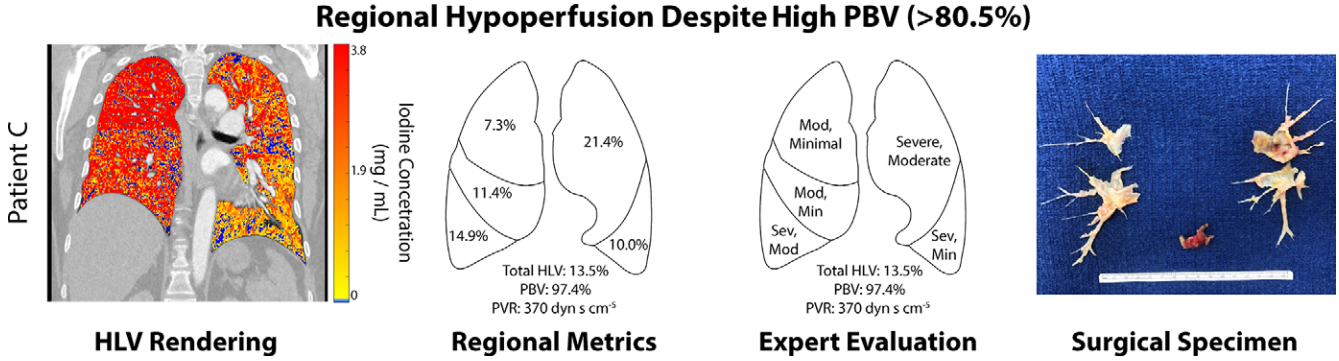

Figure 6: Use of HLV to visualize and quantify small regional perfusion deficits in a patient with high PBV. Patient C is an example of a patient with chronic thromboembolic pulmonary hypertension with high global PBV (97.4%) who underwent surgical treatment. A coronal section of the HLV visualization is shown alongside lobar evaluation of HLV and a photograph of the surgical specimen. Diminished (yellow) iodine concentration and hypoperfusion (blue) were observed on HLV mapping (left column), with the highest lobar HLV scores observed in the right lower and left upper lobes (HLV = 14.9% and 21.4%, respectively). The readers agreed regarding the relative relationship of hypoperfusion between the lobes, but reader 1 scored the hypoperfusion as more severe. The removed surgical specimen correlates with the spatial distribution of hypoperfusion seen via HLV. Note, a resected right atrial clot is present in the center of the surgical specimen. HLV = hypoperfused lung volume, Min = minimal, Mod = moderate, PBV = pulmonary blood volume, PVR = pulmonary vascular resistance, Sev = severe.

PBV and HLV are expected to provide complementary information, as HLV measures the spatial extent of impairment, while PBV is an average of parenchymal iodine concentration. As we have shown, impairments limited to a small portion of the lung may not affect the global mean iodine concentration but may result in pixels identified as being hypoperfused. We highlight how HLV mapping agrees with known CTEPH phenotypes. This could aid clinical evaluation, as the surgical technique and expertise required varies based on phenotype (30). Further, our approach to measuring HLV results in pixelwise, lobar, and global values of hypoperfusion that can be easily integrated with other patient data. Future work is planned to prospectively evaluate the use of these HLV metrics and determine an optimal way to combine PBV, HLV, and other patient data to further improve clinical assessment.

HLV correlated with preoperative and postoperative change in hemodynamic severity, in the form of PVR, in patients with surgically defined disease originating in the main or lobar artery, as well as patients with disease originating in the segmental arteries. While HLV may potentially help identify patients who are likely

to have excellent or limited response preoperatively (by identifying preoperative features of surgical success), few patients in our cohort had what would be considered limited surgical response (31,32). Thus, the ability to detect these rare events is left for future work. Cases of primarily segmental- or subsegmental-level disease are technically more challenging surgically, and patients may not receive adequate or thorough clearance except in the highest volume endarterectomy centers. As a retrospective study, we did not target enrollment of patients with these specific subtypes. Further, we did not evaluate nonsurgical cases, such as patients treated with balloon pulmonary angioplasty, medications, or a combination of treatment modalities. Therefore, the use of HLV in these cohorts should be investigated in future work.

Visual evaluations of lobar hypoperfusion by two expert readers moderately agreed with one another and with lobar HLV. Eighty-five percent (217 of 255) of lobes were scored as having the same severity or differed by only one category. Readers did not undergo specific training for this visual scoring task (outside their normal clinical training), which may explain the variation in grading. However, this variation reflects typical clinical practice in which individual readers may vary in sensitivity and specificity regarding hypoperfusion, particularly given the relatively recent clinical adoption of multienergy imaging. The moderate agreement of HLV with both readers suggests that lobar HLV could serve to support and adjudicate reader evaluations, as having an external quantitative metric has shown to improve agreement in visual assessment for other pulmonary visual assessment tasks (33). However, further studies are needed to evaluate these potential clinical uses of HLV.

The correlation between global PBV and PVR in our study ($\rho = -0.54$) was similar to that found by Takagi et al (16) ($\rho = 0.47$) and higher than that reported by Meinel et al (15) ($\rho = -0.20$). Both Takagi et al and Meinel et al reported correlations between global PBV and mPAP ($\rho = 0.48$ and -0.57, respectively), which were not observed in this study. These differences may be due to the differences in the CTEPH samples studied. In our study, all patients with CTEPH underwent PTE surgery; however, Takagi et al included patients who underwent nonsurgical treatments (medical therapy and balloon pulmonary angioplasty), and Meinel et al studied patients with CTEPH regardless of intervention. Further, we found that global HLV did not correlate with ΔCO after surgery. This may be due to the evaluation of postoperative hemodynamics while patients recovered in the intensive care unit (typically within 7 days of surgery). Long-term postoperative hemodynamic evaluation should be evaluated in future work.

Our study had several limitations. First, given the observational and retrospective nature of the study, patients in the control cohort had clinical symptoms that merited CT investigation even though they did not have pulmonary findings. It is possible that undetected pulmonary or vascular disease in control patients could have impacted iodine values and limited HLV specificity. For example, we did not exclude patients with small airways disease, which can lead to hypoperfusion. Additionally, the study did not evaluate other types of pulmonary hypertension. The study's retrospective design and the resulting effects on cohort differences were also limitations. Despite excluding patients with BMI greater than 50 kg/m^2, control patients had significantly higher BMIs than did patients with CTEPH; this may be attributed to multienergy CT being used for improved imaging of suspected PE in patients with high BMI at our institution. However, the higher BMI in the control cohort further highlights the robustness of the approach, as high BMI could decrease parenchymal iodine concentration (and increase HLV) in control patients, making it more difficult to separate CTEPH and control cases. We also observed racial and sex differences between the cohorts, which can be attributed to differences between patients referred for PTE surgery (a national referral population) and patients imaged for suspicion of PE (our local population).

Additionally, iodine concentration maps were subject to material decomposition errors, leading to negative iodine concentration values. In thoracic multienergy CT images, it is common to have highly negative pixels due to streak artifacts from regions with high contrast concentrations, such as in the superior vena cava. Additionally, motion artifacts from cardiac and diaphragmatic motion can lead to photon starvation artifacts (21,34). We aimed to minimize these artifacts by using a lower intensity threshold (–3 mg/mL iodine) to remove pixels with values likely due to artifact. Multienergy material decomposition can also have a bias in the iodine concentration. In phantom imaging studies, negative biases of –1.5 mg/mL have been reported. This bias supports our hypoperfusion threshold of 0 mg/mL as capturing pixels with poor perfusion.

Furthermore, while our study evaluated a considerable number of patients with CTEPH who underwent surgical treatment, the inclusion of more patients would improve the subgroup analysis and generalizability of this study. The study design did not control for the level of CTEPH disease removed at the time of PTE surgery or the timing of CT imaging, hemodynamic assessment, and surgery. As a result, our cohort did not include patients with disease originating in the subsegmental arteries (surgical disease level 4) and may be limited by changes between imaging and hemodynamic measurement. Thus, future investigation in a broader patient cohort reflecting all disease levels is warranted. Additionally, the single-site design reduced variability in CTEPH diagnostic and treatment criteria, and our results should be confirmed in a validation cohort, as well as at other institutions.

Another limitation was that we compared HLV and PBV with only visual evaluation by expert readers. Future work should compare HLV and PBV with detailed analysis of surgically removed specimens and evaluate changes in HLV and PBV after PTE surgery for additional clinical validation. Unfortunately, the surgical specimens we evaluated did not document whether specific vessels were open, partially obstructed, or completely obstructed. This precluded quantitative comparisons between imaging metrics and surgical findings. In future work, we aim to assess the agreement between areas detected using HLV and the presence of surgically confirmed specimens. Finally, postoperative imaging was not performed in our patients. Longitudinal multienergy CT pulmonary angiography would allow for confirmation that areas of hypoperfusion improve with surgery.

In conclusion, multienergy perfusion imaging of the lungs can be combined with lobar segmentation to automatically visualize perfusion deficits and provide pixelwise quantification of the

spatial extent of hypoperfusion. The spatial extent of hypoperfusion, global HLV, was able to separate patients with CTEPH from controls and correlated with invasive PVR and change in PVR with surgery, even in patients with surgically defined segmental disease. Lobar HLV values agreed with expert visual assessment. These findings suggest that HLV evaluation could provide quantitative imaging-derived perfusion metrics to evaluate disease progression or response either independently or when combined with other patient clinical and imaging data, warranting further investigation.

Author contributions: Guarantors of integrity of entire study, **E.B., K.H., M.M., F.C.**; study concepts/study design or data acquisition or data analysis/interpretation, all authors; manuscript drafting or manuscript revision for important intellectual content, all authors; approval of final version of submitted manuscript, all authors; agrees to ensure any questions related to the work are appropriately resolved, all authors; literature research, **E.B., M.M., F.C.**; clinical studies, **E.B., K.H., M.M., A.M., L.H., S.K., F.C., M.M., S.K.**; statistical analysis, **E.B., S.K., F.C.**; and manuscript editing, **E.B., N.K., M.M., S.K., A.H., F.C.**

Disclosures of conflicts of interest: E.B. National Institutes of Health (NIH) grant number F30HL158220, which also provided support for attending meetings and/or travel. **K.H.** No relevant relationships. **N.K.** Consulting fees from Bayer, Janssen, Merck, and United Therapeutics, paid to author; payment or honoraria for lectures, presentations, speakers bureaus, manuscript writing, or educational events from Bayer, Janssen, and Merck, paid to author; executive board member of the International CTEPH Association, a non-profit organization. **M.M.** Royalties or licenses from Wexler Surgical; consulting fees from Janssen/Actelion. **A.M.** Funded by the NIH; income related to medical education from LivaNova, Eli Lilly, ZOLL, and Jazz. **L.H.** Consultant to the Cardiovascular Research Foundation; grant support from the Radiological Society of North America. **S.K.** Deputy editor for *Radiology: Cardiothoracic Imaging*. **A.H.** Research grant from GE Healthcare, unrelated to this work; stock or stock options in Arterys, unrelated to this work. **F.C.** No relevant relationships.

References

1. Fedullo PF, Auger WR, Kerr KM, Rubin LJ. Chronic thromboembolic pulmonary hypertension. N Engl J Med 2001;345(20):1465–1472.
2. Galiè N, Humbert M, Vachiery JL, et al. 2015 ESC/ERS Guidelines for the diagnosis and treatment of pulmonary hypertension: The Joint Task Force for the Diagnosis and Treatment of Pulmonary Hypertension of the European Society of Cardiology (ESC) and the European Respiratory Society (ERS): Endorsed by: Association for European Paediatric and Congenital Cardiology (AEPC), International Society for Heart and Lung Transplantation (ISHLT). Eur Respir J 2015;46(4):903–975. [Published correction appears in Eur Respir J 2015;46(6):1855–1856.]
3. Kim NH, Delcroix M, Jais X, et al. Chronic thromboembolic pulmonary hypertension. Eur Respir J 2019;53(1):1801915.
4. Kim NH, Delcroix M, Jenkins DP, et al. Chronic thromboembolic pulmonary hypertension. J Am Coll Cardiol 2013;62(25 Suppl):D92–D99.
5. Madani M, Mayer E, Fadel E, Jenkins DP. Pulmonary endarterectomy. Patient selection, technical challenges, and outcomes. Ann Am Thorac Soc 2016;13(Suppl 3):S240–S247.
6. Fuld MK, Halaweish AF, Haynes SE, Divekar AA, Guo J, Hoffman EA. Pulmonary perfused blood volume with dual-energy CT as surrogate for pulmonary perfusion assessed with dynamic multidetector CT. Radiology 2013;267(3):747–756.
7. Kim SS, Hur J, Kim YJ, Lee HJ, Hong YJ, Choi BW. Dual-energy CT for differentiating acute and chronic pulmonary thromboembolism: an initial experience. Int J Cardiovasc Imaging 2014;30(Suppl 2):113–120.
8. Masy M, Giordano J, Petyt G, et al. Dual-energy CT (DECT) lung perfusion in pulmonary hypertension: concordance rate with V/Q scintigraphy in diagnosing chronic thromboembolic pulmonary hypertension (CTEPH). Eur Radiol 2018;28(12):5100–5110.
9. Dournes G, Verdier D, Montaudon M, et al. Dual-energy CT perfusion and angiography in chronic thromboembolic pulmonary hypertension: diagnostic accuracy and concordance with radionuclide scintigraphy. Eur Radiol 2014;24(1):42–51.
10. Koike H, Sueyoshi E, Sakamoto I, Uetani M, Nakata T, Maemura K. Correlation between lung perfusion blood volume and SPECT images in patients with chronic thromboembolic pulmonary hypertension by balloon pulmonary angioplasty. Clin Imaging 2018;49:80–86.
11. Thieme SF, Becker CR, Hacker M, Nikolaou K, Reiser MF, Johnson TRC. Dual energy CT for the assessment of lung perfusion--correlation to scintigraphy. Eur J Radiol 2008;68(3):369–374.
12. Kunihiro Y, Okada M, Matsunaga N, et al. Dual-energy perfusion CT of non-diseased lung segments using dual-source CT: correlation with perfusion SPECT. Jpn J Radiol 2013;31(2):99–104.
13. Nallasamy N, Bullen J, Karim W, Heresi GA, Renapurkar RD. Evaluation of vascular parameters in patients with pulmonary thromboembolic disease using dual-energy computed tomography. J Thorac Imaging 2019;34(6):367–372.
14. Hoey ETD, Mirsadraee S, Pepke-Zaba J, Jenkins DP, Gopalan D, Screaton NJ. Dual-energy CT angiography for assessment of regional pulmonary perfusion in patients with chronic thromboembolic pulmonary hypertension: initial experience. AJR Am J Roentgenol 2011;196(3):524–532.
15. Meinel FG, Graef A, Thierfelder KM, et al. Automated quantification of pulmonary perfused blood volume by dual-energy CTPA in chronic thromboembolic pulmonary hypertension. Rofo 2014;186(2):151–156.
16. Takagi H, Ota H, Sugimura K, et al. Dual-energy CT to estimate clinical severity of chronic thromboembolic pulmonary hypertension: Comparison with invasive right heart catheterization. Eur J Radiol 2016;85(9):1574–1580.
17. Koike H, Sueyoshi E, Sakamoto I, Uetani M, Nakata T, Maemura K. Comparative clinical and predictive value of lung perfusion blood volume CT, lung perfusion SPECT and catheter pulmonary angiography images in patients with chronic thromboembolic pulmonary hypertension before and after balloon pulmonary angioplasty. Eur Radiol 2018;28(12):5091–5099.
18. Atwi NE, Smith DL, Flores CD, et al. Dual-energy CT in the obese: a preliminary retrospective review to evaluate quality and feasibility of the single-source dual-detector implementation. Abdom Radiol (NY) 2019;44(2):783–789.
19. Hahn LD, Hall K, Alebdi T, Kligerman SJ, Hsiao A. Automated deep learning analysis for quality improvement of CT pulmonary angiography. Radiol Artif Intell 2022;4(2):e210162.
20. Hasenstab K, Yuan N, Retson T, et al. Automated CT staging of chronic obstructive pulmonary disease severity for predicting disease progression and mortality with a deep learning convolutional neural network. Radiol Cardiothorac Imaging 2021;3(2):e200477. [Published correction appears in Radiol Cardiothorac Imaging 2022;4(1):e219002.]
21. Machida H, Tanaka I, Fukui R, et al. Dual-energy spectral CT: various clinical vascular applications. RadioGraphics 2016;36(4):1215–1232.
22. Contijoch F, Wong D, Igata S, et al. Association between preoperative dynamic measures of vascular load and postoperative hemodynamics in patients with chronic thromboembolic pulmonary hypertension after pulmonary thromboendarterectomy. Ann Am Thorac Soc 2021;18(3):551.
23. Hanley JA, McNeil BJ. The meaning and use of the area under a receiver operating characteristic (ROC) curve. Radiology 1982;143(1):29–36.
24. DeLong ER, DeLong DM, Clarke-Pearson DL. Comparing the areas under two or more correlated receiver operating characteristic curves: a nonparametric approach. Biometrics 1988;44(3):837–845.
25. Li J, Fine J. On sample size for sensitivity and specificity in prospective diagnostic accuracy studies. Stat Med 2004;23(16):2537–2550.
26. Portney LG, Watkins MP. Foundations of clinical research: applications to practice. 3rd ed. Upper Saddle River, NJ: Pearson/Prentice Hall, 2009.
27. Williams EJ. The comparison of regression variables. J R Stat Soc Ser B Methodol 1959;21(2):396–399.
28. Steiger JH. Tests for comparing elements of a correlation matrix. Psychol Bull 1980;87(2):245–251.
29. Koo TK, Li MY. A guideline of selecting and reporting intraclass correlation coefficients for reliability research. J Chiropr Med 2016;15(2):155–163. [Published correction appears in J Chiropr Med 2017;16(4):346.]
30. D'Armini AM, Morsolini M, Mattiucci G, et al. Pulmonary endarterectomy for distal chronic thromboembolic pulmonary hypertension. J Thorac Cardiovasc Surg 2014;148(3):1005–1011, 1012.e1–1012.e2; discussion 1011–1012.
31. Madani MM. Surgical treatment of chronic thromboembolic pulmonary hypertension: pulmonary thromboendarterectomy. Methodist DeBakey Cardiovasc J 2016;12(4):213–218.
32. Mahmud E, Madani MM, Kim NH, et al. Chronic thromboembolic pulmonary hypertension: evolving therapeutic approaches for operable and inoperable disease. J Am Coll Cardiol 2018;71(21):2468–2486.
33. Retson TA, Hasenstab KA, Kligerman SJ, et al. Reader perceptions and impact of AI on CT assessment of air trapping. Radiol Artif Intell 2021;4(2):e210160.
34. Parakh A, Lennartz S, An C, et al. Dual-energy CT images: pearls and pitfalls. RadioGraphics 2021;41(1):98–119.